Biopolymer patches for the simultaneous incorporation of local anesthetic and anti-inflammatory drugs

Dorinel Okolišan[1] · Titus Vlase[1,2] · Gabriela Vlase[1,2] · Ionela-Amalia Bradu[1,2] · Alexandru Pahomi[1] ·
Anamaria Matichescu[3]

Abstract

This study presents a novel type of biopolymer patches in which anti-inflammatory drugs and amide-type anesthetics were simultaneously incorporated. Since the biopolymer matrix is composed of k-carrageenan, hydroxyethyl cellulose, and glycerol, as a plasticizer, the resulting patches have an elasticity and a "stickiness" that can be exploited in the field of transdermal delivery of drugs. Combinations of anesthetic and anti-inflammatory drugs resulted in twenty patches with a unique and distinct physical appearance. Furthermore, as indicated by FTIR, TG/DTG, and DSC analysis data, none of the active substances affects the integrity of the biopolymer matrix; instead, they influence the $T_{melting}$ of the patch matrix, either in its value increase or decrease.

Introduction

Although the oral administration of therapeutic agents is regarded as the most popular and convenient method, it presents some disadvantages, including hydrolysis in the stomach, enzymatic digestion, and metabolism in the liver, due to which the orally administered drug may be eliminated prematurely before it reaches systemic circulation [1]. Therefore, an alternative to this general method of administration is a drug delivery system that aims to deliver the active principle in such a way as to ensure the achievement of well-established therapeutic effects [2]. In a drug delivery system, the carrier of the therapeutic agent is always biodegradable and biocompatible, whereas the desired therapeutic effect can be achieved with a smaller amount of drug, and once the agent has been delivered, the carrier must be easily removed [3]. A drug delivery system is designed in such a way that it must overcome the side effects associated with a drug (from conventional routes) to increase the therapeutic effect of the active principle, by means of improving the chemical stability and solubility of the therapeutic agent [4]. One such system, which overcomes the limitations of conventional formulations, but ensures a better bioavailability of the drug and at the same time contributes to the reduction in the frequency of doses, is the transdermal delivery of drugs (TDD) [5]. The greatest advantages of this delivery system are the ability to overcome gastrointestinal side effects and the hepatic elimination process, thus ensuring a controlled release of the active principle in the bloodstream over a longer period of time [6].

Biopolymers are organic compounds whose fundamental building blocks can be either simple component units, termed monomers, or complex units, often known as repeating units [7]. Depending on the nature of the building block, biopolymers can be classified into three major categories: (1) polynucleotides—when the skeleton is made up of at least 13 nucleotide monomers; (2) polypeptides—where monomeric units are amino acids; and (3) polysaccharides—when the

✉ Titus Vlase
titus.vlase@e-uvt.ro

1   Research Centre for Thermal Analysis in Environmental Problems, West University of Timisoara, Pestalozzi Street 16, 300115 Timisoara, Romania

2   ICAM - Advanced Environmental Research Institute, West University of Timisoara, Oituz No. 4, Timisoara, Romania

3   Department of Preventive Dentistry, Community and Oral Health, Faculty of Dental Medicine, University of Medicine and Pharmacy ''Victor Babes'', Spl. Tudor Vladimirescu No. 14A, 300173 Timisoara, Romania

backbone is made up of saccharide units [8]. These natural molecules can organize themselves into hierarchical structures since the monomeric units, from the primary structures, can arrange themselves to form a secondary structure which in turn can sometimes take on the appearance of a three-dimensional framework, thus creating a tertiary structure [9]. As molecules that are produced by cells of living organisms, they present a series of properties, such as biodegradability, biocompatibility, and antibacterial properties [8], thanks to which they have found a wide range of applications including the cosmetic industry, the food additive industry, wastewater treatment, packaging materials, and perhaps most importantly as a basis for various medical materials [10].

From a chemical point of view, carrageenan is a sulfated hydrophilic polysaccharide that has a general anionic character, as a result of the presence of the sulfate group on its skeleton [11]. As it is known, the term "Carrageenan" does not refer to a specific compound but to a class of compounds whose basic skeleton consists of alternating β-D-galactopyranose and α-D-galactopyranose units or 3,6-anhydrogalactopyranose units [12]. Depending on the degree of sulfation of galactose unit and the position of sulfate groups, they can be classified into six groups, as follows: ι—iota, κ—kappa, λ—lambda, μ—mu, ν—nu, and θ—theta carrageenan [13]. λ-Carrageenan does not gel, while the gelation of κ- and ι-carrageenan is induced by the presence of specific ions; thus, κ- forms rigid gels with potassium ions while ι- forms soft and elastic gels with calcium ions [14]. Among all these types, the most used form is k-carrageenan which, due to its excellent gelation property, the thermoreversibility of its gels, but also the fact that its gels are compact, rigid, and transparent, is an excellent raw material for a variety of biopolymer films [15]. Moreover, these properties make it an excellent transport vehicle for active principles in some drug delivery systems, where it is used as an "embedding" material because it can provide a more stable environment for the active principle thus maximizing the value of the therapeutic agent [16].

Due to their ability to eliminate the sensation of pain, local anesthetics have enjoyed increasing popularity since their introduction in the late nineteenth century, so that today they are regularly used either in the blockage of peripheral nerves or in intravenous administration, thus ensuring patient compliance [17]. The chemical structure of local anesthetics consists of a lipophilic portion, a substituted benzene ring, linked to the hydrophilic portion, usually a tertiary amine, through a linkage group that can be an amide or an ester [18]. Therefore, depending on the nature of the linkage group, they are divided into two categories, amide-type anesthetics, and ester-type anesthetics [19]. In general, local anesthetics are weak bases [20] and their absorption and distribution depend on the pKa value, hydrophobicity, and chemical structure of the local anesthetic as well as on the site and mode of administration of these drugs [21]. Adverse effects associated with local anesthetics are frequent, while allergic effects are extremely rare [22], being associated with their metabolic product, namely p-aminobenzoic acid [23]. Therefore, the decomposition of ester-type anesthetics takes place under the influence of plasma pseudocholinesterase, the metabolic products being excreted in the urine, while amide-type anesthetics are metabolized in the liver, which requires special attention when administered to patients with kidney problems [23]. In this study, five amide anesthetics were used for incorporation into the biopolymer matrix: lidocaine, mepivacaine, bupivacaine, ropivacaine, and articaine. The chemical structure of these local anesthetic drugs is shown in Fig. 1.

Starting from Hippocrates' description of the treatment of fever and pain with willow bark extract, and the first synthesis of an NSAID (acetylsalicylate in 1897), a multitude of researchers have devoted considerable effort to "gift mankind" a large number of compounds exhibiting these therapeutic effects. [24]. As a result, there are two broad classes of anti-inflammatory drugs, namely phospholipase inhibitors, corticosteroid drugs, and nonsteroidal anti-inflammatory drugs or NSAIDs, which are cyclo-oxygenase inhibitors [25]. Regardless of their mechanism of action, all anti-inflammatory drugs can reduce fever and inflammation as well as pain, whether mild or moderate, except for pain associated with visceral organs [26]. Since NSAIDs can non-selectively inhibit both COX isoforms, COX-2 selective NSAIDs (COXIBs) have been developed over the years, which can avoid the adverse effects associated with COX-1 inhibition, such as decreased gastric cytoprotective effect and hepatic failure. [27]. The five anti-inflammatory drugs used in the preparation of biopolymer patches are sodium diclofenac, dexketoprofen trometamol, meloxicam, and dexamethasone phosphate, and the chemical structure of these therapeutic agents is shown in Fig. 1.

As it was reported in a study from 2023 [37], excipients can directly influence the stability of the active substance, which can be evidenced by means of thermogravimetric analysis. Moreover, some excipients, such as cellulose derivatives, can affect the crystallinity of the active substance, an effect that can be observed by DSC analysis [38]. This study aims to obtain biopolymer patches in which anti-inflammatory drugs and local anesthetics will be incorporated simultaneously. Thus, each local anesthetic chosen to be studied is combined in turn with each anti-inflammatory drug. FTIR, TG/DTG, and DSC techniques were chosen for the analysis of the patches, which can provide us with information regarding the successful incorporation of the active substances as well as the behavior and thermal stability of the synthesized patches.
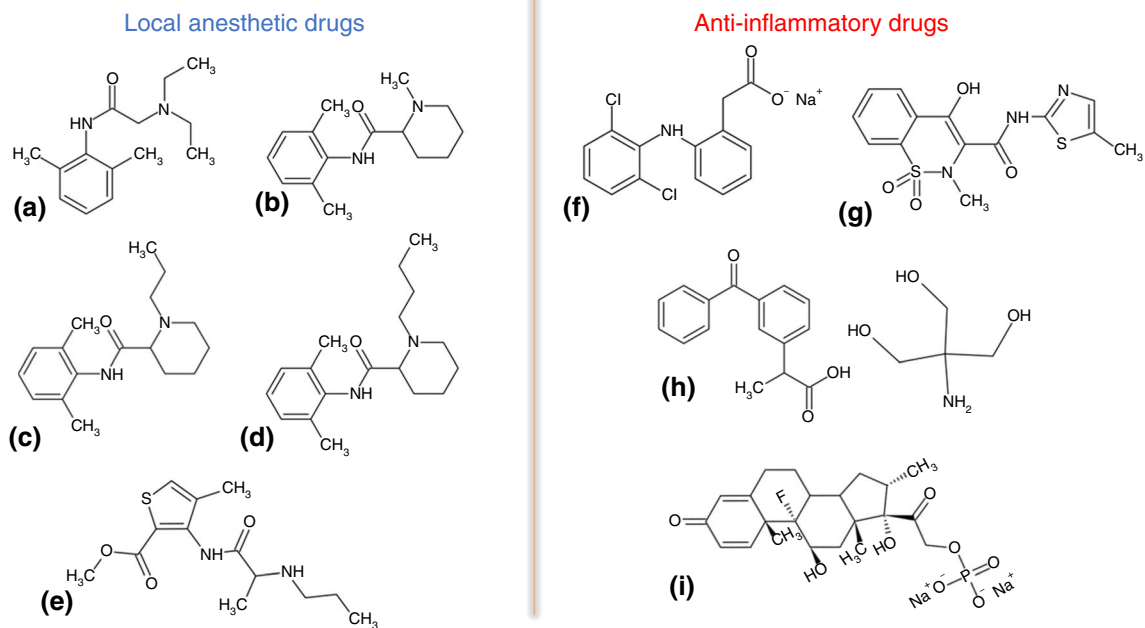
Fig. 1 Chemical structure of: **a** lidocaine (adapted from [28]); **b** mepivacaine (adapted from [29]); **c** ropivacaine (adapted from [30]); **d** bupivacaine (adapted from [31]); **e** articaine (adapted from [32]); **f** sodium diclofenac (adapted from [33]); **g** meloxicam (adapted from [34]); **h** dexketoprofen trometamol (adapted from [35]); **i** dexamethasone phosphate (adapted from [36])

Materials and methods

Materials

The basic constituents of patches are κ-carrageenan by Acros Organics (Geel, Belgium) CAS: 11114-20-8; hydroxyethyl cellulose, CAS: 9004-62-0 (Sigma-Aldrich Chemie GmbH, Taufkirchen, Germany); and glycerol, as a plasticizer, CAS: 56-81-5, sold by CHIMREACTIV (Ion Creangă, Romania).

The local anesthetics used in this study are:

- *Lidocaine*: (40 mg mL^{-1}) marketed as *Xilină* by *S.C. ZENTIVA S.A (Bucureşti, Romania);*
- *Mepivacaine*: (30 mg mL^{-1}) commercialized as *3 M™ Mepivastesin™ (3 M Deutschland GmbH, Neuss, Germany);*
- *Ropivacaine*: (10 mg mL^{-1}) produced by *Fresenius Kabi (Ghimbav, Romania);*
- *Bupivacaine:* (5 mg mL^{-1}) provided as Marcaine Spinal and produced by Astra Zeneca *(CENEXI, Fontenay-sous-Bois, France)*;
- *Articaine*: (40 mg mL^{-1}) marketed as 3 M™ Ubistesin™ Forte *(3 M Deutschland GmbH, Neuss, Germany)*.

The anti-inflammatory drugs used in the study are:

- *Sodium diclofenac:* (25 mg mL^{-1}) marketed as *Refen™ by STADA HEMOFARM*:
- *Dexketoprofen trometamol:* (25 mg mL^{-1}) commercialized as *Tador™ by MENARINI I.;*
- *Meloxicam:* (10 mg mL^{-1}) produced by Rompharm;
- *Dexamethasone phosphate:* (4 mg mL^{-1}) marketed as *Dexametazonă* and also produced by *Rompfarm.*

Methods

In a suitable Berzelius beaker, the required amount of glycerol was weighed (as 47% of the dry components), over which the two polysaccharides (dry components), κ-carrageenan, and hydroxyethyl cellulose (in a mass ratio of 1:1, w/w) were added, and finally, everything was covered with 10 mL of distilled water. For homogenization, the solution thus prepared was placed for 10 min on a magnetic stirrer at 500 rpm and a constant temperature of 75 °C until all the components were completely dissolved. Once a homogeneous solution was obtained, it was poured into Petri dish (d = 5 cm) and left to dry at an ambient laboratory temperature of 20 °C. To obtain patches with active substances, a calculated volume is taken from the stock solution over which the necessary volume of drugs is added so that there is a ratio of 4:1:1, between the components

of the biopolymer patch base and the active substances. Therefore, the composition of the resulting patches is as follows: 63 mg (patch base), 15.75 mg of local anesthetic, and 15.75 mg of the anti-inflammatory drug (in accordance with the established ratio, 4:1:1).

FTIR

Data collection was done after 20 recordings at a resolution of 4 cm^{-1}, in the range of 4000–400 cm^{-1} on Shimadzu AIM-9000, FT-IR Spectrometer IRTracer-100 with ATR.

TG/DTG

Thermal analysis was conducted using METTLER TOLEDO Thermogravimetric Analyzer, model TGA/DSC3^{+}, in the temperature range of 25–500 °C, with a heating rate of 10 °C min^{-1}, and in an dynamic air atmosphere (synthetic air 5.0 SIAD with flow 50 mL min^{-1}).

DSC

Samples were analyzed on METTLER TOLEDO DSC 3 +, in an dynamic air atmosphere (synthetic air 5.0 SIAD with flow 50 mL min^{-1}) and with a heating rate of 10 °C min^{-1}, within a temperature range of 25–500 °C.

Results and discussion

Obtaining biopolymer patches

Control patch synthesis

According to the synthesis methodology described earlier, a control patch (Fig. 2) was also synthesized so that it could be compared with the active substance patches. Thus, 64 h

Fig. 2 Control patch appearance (CCG)

at a temperature of 20 °C was needed to dry the patch, so that it could be detached from the Petri dish without compromising its integrity. Moreover, it should be noted that after 48 h of drying, the patch was turned to the opposite side, to ensure uniform drying. Thanks to the glycerol present in the composition of this patch, its detachment was extremely easy; moreover, the hydroxyethyl cellulose gives the patch a rather enhanced elasticity. In addition, glycerol "gives" the patch a sticky character that can be "exploited" in transdermal delivery systems. As shown in Fig. 2, the resulting patch has a smooth, glossy surface, and due to its stickiness at the moment of its handling, some creases were created, which by stretching can return to the initial state of the patch (before its manipulation).

Synthesis of patches with active substances

Following the synthesis of patches with active substances, twenty patches were obtained in which each local anesthetic was combined, in turn, with each anti-inflammatory drug. It should be noted that the ratio of active substances was 1:1 (w/w) while maintaining the already established ratio of 4:1:1 for hydrogel base and active substance. Therefore, the obtained patches have a different physical appearance because of different combinations of active substances (Table 1).

a. Patches in which articaine was combined with anti-inflammatory drugs.

As a result of the study, four patches were obtained in which, along with articaine, four anti-inflammatory drugs were incorporated. As given in Table 1, two completely transparent patches were obtained (CCGAR and CCGAT), one opaque (CCGAD), and only one colored (CCGAM), due to the straw-yellow meloxicam solution that was used in the preparation of this patch. The opacity of the CCGAD patch is due to dexamethasone, which crystalizes as the solvent evaporates and becomes dispersed in the hydrogel matrix. Although the CCGAM patch is elastic, its elasticity is lower compared to the other obtained films. The CCGAT patch is the stickiest, which made it difficult to peel it and contributed to the formation of irregular wrinkles upon its removal from the Petri dish. All obtained patches have a sticky character, and good adhesion on the skin, due to the glycerol present in the hydrogel matrix. In addition, hydroxyethyl cellulose contributes to the elasticity of these patches.

b. Patches in which lidocaine was combined with anti-inflammatory drugs.

Depending on the combination of medicinal substances, the obtained patches have a physical appearance that varies from patch to patch. Thus, two

Table 1 Physical appearance of patches in which combinations of local anesthetics and anti-inflammatory drugs have been incorporated

+	Sodium Diclofenac	Dexketoprofen trometamol	Dexamethasone phospahte	Meloxicam
Lidocaine	*CCGLR*	*CCGLT*	*CCGLM*	*CCGLD*
Articaine	*CCGAR*	*CCGAT*	*CCGAM*	*CCGAD*
Bupivacaine	*CCGBR*	*CCGBT*	*CCGBM*	*CCGBD*
Ropivacaine	*CCGRR*	*CCGRT*	*CCGRM*	*CCGRD*
Mepivacaine	*CCGMR*	*CCGMT*	*CCGMM*	*CCGMD*

completely transparent patches (CCGLR and CCGLT), a yellowish patch (CCGLM), and an opaque patch (CCGLD) were obtained, according to the samples shown in Table 1. Even if the same synthesis method was used, not all obtained patches show elasticity that is in accordance with the one that control (CCG) poses. As can be seen from the images in Table 1, due to the folds that appear on their surface, during handling, the CCGLR patch shows a very pronounced sticky character, followed by the CCGLT and finally, the CCGLM and CCGLD patches. Thus, depending on this physical property, the removal of the patch from the Petri dish and its handling is more or less difficult. CCGLD and CCGLM patches have the appearance of baking paper with a smooth and dry, but readily waxy surface when touched with a fingertip. CCGLR and CCGLT films, elastic and sticky, behave like a parafilm, and they have a certain mechanical tensile strength and an excellent ability to "stick" to the skin surface, properties that are due to both hydroxyethyl cellulose and the plasticizer, glycerol.

c. Patches in which bupivacaine was combined with anti-inflammatory drugs.

As can be seen from the sample images shown in Table 1, two semitransparent patches (CCGBR and CCGBT), one completely opaque (CCGBD), and only one colored (CCGBM) were obtained. In the case of the CCGBD film, its opacity is due to bupivacaine but also dexamethasone phosphate (very finely dispersed crystals in the hydrogel matrix), whereas in the case of the CCGBT and CCGBR, their semi-transparency is the result of the presence of bupivacaine. Elasticity is a property that the patches obtained from this study also possess, except the CCGBD which is much more brittle than the CCGBM, CCGBR, CCGBT patches, and even the CCGLD and CCGAD. Although glycerol was added as a plasticizer to ensure elasticity, it cannot fully exert this property due to the crystallization of bupivacaine and dexamethasone, thus resulting in increased fragility of the CCGBD patch. It should be noted that the CCGBM has a yellowish color due to the meloxicam solution that was used in its synthesis and that the CCGBT is extremely "sticky" which contributed to the formation of irregular wrinkles on its surface during handling.

d. Patches in which ropivacaine was combined with anti-inflammatory drugs.

Following this study, combinations of ropivacaine and anti-inflammatory drugs resulted in four patches of which two were semitransparent (CCGRR and CCGRT) and, as expected, one was completely opaque (CCGRD) and one was yellowish (CCGRM). The semitransparent films show no trace of the crystallized active substance. Even in the absence of substance crystals, this semi-transparency could be attributed to ropivacaine, assuming that it is uniformly dispersed in the polysaccharide matrix of the obtained film.

In the case of the CCGRM and CCGRD patches, although elastic, they cannot be compared with the other two patches neither by their opacity nor by their degree of dryness. Although the same drying conditions were applied for all patches, the CCGRM and CCGRD samples show a higher degree of dryness than the CCGRR and CCGRT samples, which directly facilitates their detachment from the Petri dish. As expected, in the case of the CCGRD sample which has the appearance of crepe paper, but is "sticky" to the touch, the crystallization of dexamethasone phosphate increases its fragility but not to such a great extent as in the case of the CCGBD patch where the integrity of the polysaccharide matrix has been affected.

e. Patches in which mepivacaine was combined with anti-inflammatory drugs

Following the work methodology described above, four biopolymer patches were obtained in which combinations of mepivacaine with the anti-inflammatory

drugs chosen to be studied were incorporated. Thus, even if the drying time and conditions were respected, depending on the combination of active substances, the obtained patches present a different physical appearance (Table 1); namely, meloxicam contributes to the coloring of the obtained patch, giving it a yellowish tinge (CCGMM), two completely transparent patches (CCGMR and CCGMT) and a patch that, once again, presents an opacity as a result of the crystallization of the incorporated anti-inflammatory drug (CCGMD).

The two transparent samples, CCGMR and CCGMT, exhibit an elasticity that, when handled, can be compared to that of the CCG control film. Visually, patches appear to be identical, but upon closer examination, we can see that they present a different degree of dryness which, in addition to touching them, can also be deduced from light reflection on their surface. Thus, the CCGMR patch, elastic and sticky, is much drier than the CCGMT patch, even though the drying conditions were the same. The CCGMM and CCGMD samples, which due to the incorporated anti-inflammatory drugs have a higher degree of dryness than all obtained patches, do not show such a pronounced "sticky" character, and therefore, their peeling and handling were easier.

FTIR

To facilitate the "deciphering" of the FTIR spectrum of the control patch (CCG), since the patch is composed of two different biopolymers, it was considered necessary to compare it with the FTIR spectrum of the constituent biopolymers (Fig. 3a). The biopolymer matrix's constituents, being polysaccharides, present a multitude of C-H, C–OH, and C–O–C bonds, which appear in the FTIR spectrum as follows: the stretching vibrations of the O–H bond at 3307 cm^{-1} and those of the C-H bond at 2893 cm^{-1}. Moreover, since many hydroxyl groups are attached to the saccharide units, at 1053 cm^{-1} appears the most intense peak of the FTIR spectrum, due to the stretching vibrations of the C–OH bonds. In addition, the saccharide units being linked by the glycosidic bond, the -C–O–C- bond was expected to exhibit vibration, which in the case of HEC appears at 870 cm^{-1} and at 891 cm^{-1} for κ-carrageenan. As sulfated galactan, κ-carrageenan presents characteristic vibrations, among which are the S=O stretching vibration at 1224 cm^{-1} and the stretching vibrations between the carbon of the saccharide unit and the oxygen atom of the sulfate group at 810 cm^{-1}, νC-OSO$_3$H. For HEC, it can be observed that it presents a peak at 1269 cm^{-1} which is due to the deformation of -CH$_2$- from an aliphatic chain, in this case to the two -CH$_2$- from the hydroxyethyl fragment linked to C$_6$ of the saccharide unit. From a theoretical point of view, we can say that this peak can be considered as a witness that can
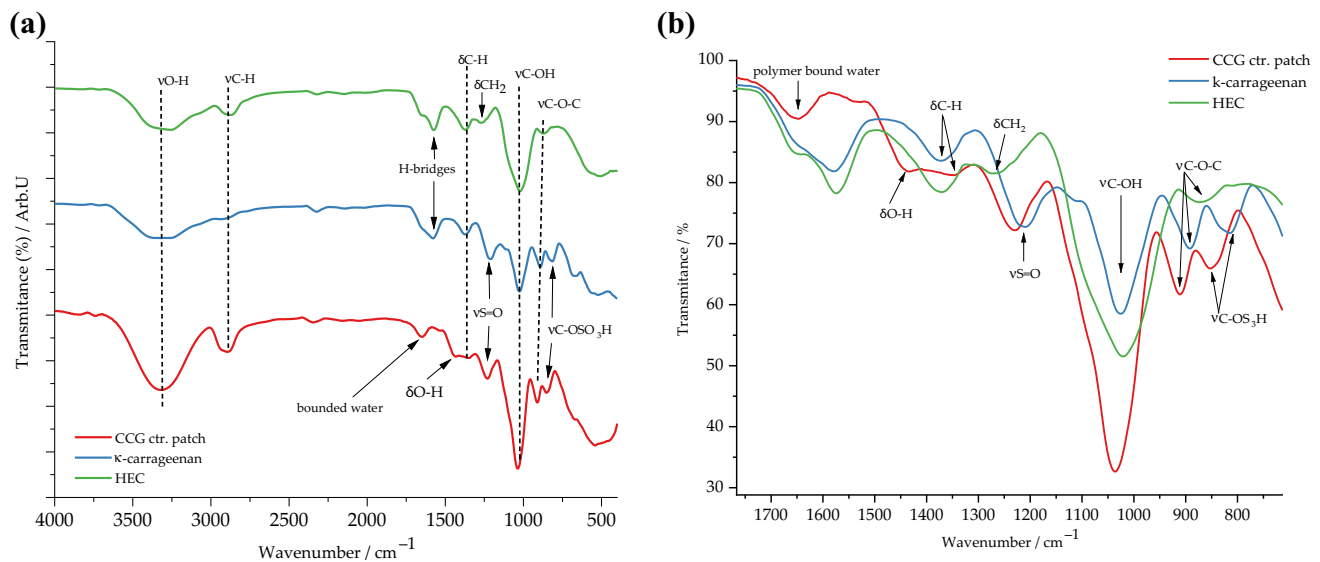
Fig. 3 **a** Comparison of FTIR spectra of control patch (CCG), κ-carrageenan and hydroxyethyl cellulose (HEC); **b** highlighting the fingerprint area of the control patch

indicate the success of obtaining cellulose derivatives, more precisely cellulose ethers (with a small alkyl fragment). Both biopolymers also present C-H deformation vibrations at 1369 cm^{-1} and a peak at 1575 cm-1 which is attributed to hydrogen bridges, basically to H bonds between the polymer chains of these polysaccharides.

For the control patch (Fig. 3b), the presence of HEC does not induce structural changes in k-carrageenan because its fingerprint area appears unaltered, even though the νC-SO$_3$H peak appears at a slightly higher wave number, at 852 cm^{-1}, than is the case for pure κ-carrageenan (810 cm^{-1}). If we were to compare the intensities of the peaks around 1300–800 cm^{-1} (both for the control patch, HEC, and κ-carrageenan), we can see that the peaks of the CCG sample show a higher intensity than is the case with the matrix components (by oneself). Each of these components brings C–OH bonds to the system, and as it is well known that the intensity of the peak is dependent on the number of bonds capable of absorbing IR light at a specific wavenumber, the intensity of the peak corresponding to νC-OH is thus more pronounced in the control patch, as shown in Fig. 3b. Moreover, the peak for δCH$_2$ in HEC is not visible in the CCG sample because it is covered by the νS$=$O peak from κ-carrageenan. The peak for δC-H is still visible but becomes shifted to 1342 cm^{-1}, while for CCG sample, at 1436 cm^{-1} a new peak appears, which is attributed to δO-H. In addition, for the control patch, the peak attributed to hydrogen bridges disappears, but at 1647 cm^{-1} a peak appears indicating that there is polymer bound water in the patch, which was expected because, during the drying process, a small amount of solvent becomes "trapped" into the biopolymer matrix.

For patches incorporating combinations of anesthetics and anti-inflammatory drugs, the FTIR analysis results were grouped and represented graphically according to the anti-inflammatory drug present in the patch, to avoid reporting repetitive information for local anesthetics. Thus, the FTIR data of the 20 patches were grouped into four graphs as follows: patches containing dexamethasone phosphate and local anesthetics (LA) in Fig. 4a; patches containing meloxicam + LA (Fig. 4b); patches with dexketoprofen trometamol + LA (Fig. 4c); and patches with sodium diclofenac + LA (Fig. 4d). In all obtained patches, the presence of local anesthetics can be highlighted by the appearance of the following signals: The peak for νC$=$O from the amide linkage, between the lipophilic and hydrophilic portion, appears at 1678 cm^{-1}; the peak of the amide band II appears at 1589 cm^{-1} and is due to the deformation of the N–H bond; the peak for skeletal vibration of the lipophilic portion, due to νC$=$C and ν=C-H, appears at 1446 cm^{-1}; and finally, the νC-N peak of the amide bond appears at 1259 cm^{-1}. Therefore, these peaks can be considered as witnesses for the presence of local anesthetics in the obtained patches, and thus, we can say that these LA have been successfully incorporated into the biopolymer matrix. Looking at the 1100–800 cm^{-1} area, it can be seen that characteristic peaks from κ-carrageenan do not disappear, which indicates that none of the two classes of active substances induces changes in the molecular structure of this biopolymer. For hydroxyethyl cellulose, although we know that it is present in the patch matrix, the FTIR spectra do not show the νCH2 peak of the hydroxyethyl moiety because its absorption range overlaps with the νC-N absorption range of local anesthetics. Both biopolymers of the patch matrix contribute
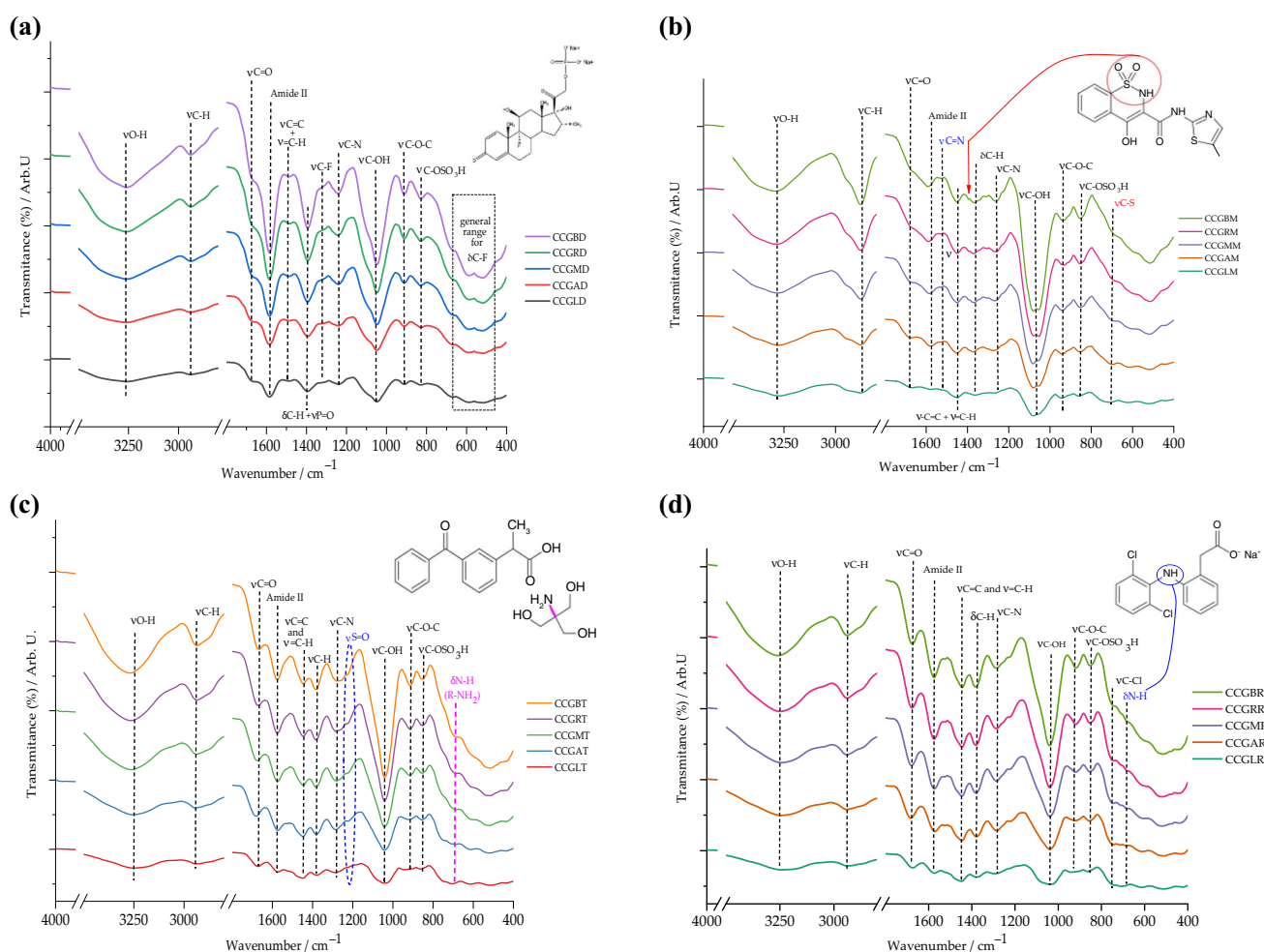
Fig. 4 FTIR data for **a** patches containing dexamethasone phosphate and local anesthetics (LA); **b** patches containing meloxicam+LA; **c** patches with dexketoprofen trometamol; and **d** patches with sodium diclofenac+LA

to the peaks for νO-H at 3280 cm^{-1}, νC-H at 2877 cm^{-1}, δC-H at 1359 cm^{-1}, νC-OH at 1053 cm^{-1}, and νC-O-C at 935 cm^{-1}.

For the patches in which dexamethasone phosphate and local anesthetics were incorporated, the FTIR spectrum is presented in Fig. 4a. The presence of dexamethasone phosphate in the analyzed patches can be highlighted by the appearance of the peak for νC-F at 1323 cm^{-1} and by the area contained within the rectangle, which corresponds to the domain in which the deformations of this interatomic bond take place. Moreover, since dexamethasone possesses a phosphate group attached to the glucocorticoid fragment, the stretching vibrations of the P=O bond contribute to the intensification of the peak intensity corresponding to δC-H since these two bond types present the same IR light absorption range. Moreover, the two carbonyl groups of dexamethasone phosphate intensify the νC=O peak, and as a result, the peak appears as a "side shoulder" of the amide band II.

From the FTIR spectra presented in Fig. 4b, for the patches in which LA was incorporated along with meloxicam, several peaks can be highlighted and attributed to the anti-inflammatory drug. On a closer look at the peak attributed to C-H bond bending vibrations, it can be seen that an extremely small "side shoulder" appears at $\approx$1392 cm^{-1}, whereby the sulfonamide moiety confirms its presence due to ν_{as} O=S=O. Another peak associated with the anti-inflammatory drug, but with a rather low intensity, is the one at 1525 cm^{-1} which originates from the stretching vibrations of the C=N bond of the thiazole fragment. Moreover, at 694 cm^{-1} a peak can be observed due to C-S bond vibrations, both from the thiazole fragment and from the 4-hydroxy-1λ^6,2-benzothiazine-1,1(2H)-dione fragment. Thus, the appearance of these peaks confirms with certainty the successful incorporation of meloxicam into the synthesized patches.

As for the patches with dexketoprofen trometamol and local anesthetics, their FTIR spectra are shown in Fig. 4c. To

highlight the success of incorporating dexketoprofen in the synthesized patches, we can use the following information: the two benzene rings contribute to the intensity of the peak at 1444 cm^{-1} because they bring to the system addition of C=C and =C-H bonds; the carbonyl connecting the two benzene rings appears and intensifies the νC=O peak at 1670 cm^{-1}; and deformations of the N–H bond in the trometamol fragment contribute to the appearance of the corresponding peak at 700 cm^{-1}. One thing should be noted, namely, the fact that in the case of patches with meloxicam, at 1220 cm^{-1} one can see the νS=O peak from κ-carrageenan, as a "side shoulder" of the νC-N peak.

For diclofenac sodium patches and local anesthetics, the FTIR spectra are presented in Fig. 4d. Thus, the peak for the stretching vibrations of the C–Cl bond at 746 cm^{-1} and the peak at 678 cm^{-1} for the bending vibrations of the N–H bond, which connects the two benzene rings, can be attributed to diclofenac sodium. Moreover, the two benzene rings contribute to the peak intensity for νC=C and νC-H, from 1444 cm^{-1}. Although the CO_2^- stretching vibrations should be visible in the FTIR spectra of diclofenac patches, because this compound is in salt form, they are being "covered" by the skeletal vibrations of the benzene ring from both local anesthetics and the anti-inflammatory drug. Also, the carbonyl of the carboxylic moiety increases the intensity of the νC=O peak. Finally, at 1219 cm^{-1} the corresponding νS=O peak from κ-carrageenan can be seen, again as a "side shoulder" of the νC-N peak.

TG/ DTG

Since the FTIR analysis revealed the successful incorporation of the local anesthetic and anti-inflammatory drugs, the determination of the stability and thermal behavior of the obtained patches as well as of the incorporated active substances is more than necessary. Thus, in the following subsections, the results of the thermogravimetric analysis for the twenty patches will be presented.

a. Patches in which articaine was combined with anti-inflammatory drugs.

The CCGAD patch undergoes three thermal decomposition processes between 38.12–433.50 ℃, resulting in a total mass loss of 63.89%. The first process, occurring at 38.12–91.48 ℃, accounts for 5.01% mass loss due to moisture. The second process, at 119.46 ℃, has a mass loss of 3.13% from intermolecular water loss. The last process results in a mass loss of 55.75% from the degradation of the patch matrix at ≈140–220 ℃ and the decomposition of active substances at ≈240 ℃, ending at 433.50 ℃. The CCGAM patch undergoes thermal decomposition in three stages according to its DTG curve. The first stage involves moisture loss at 64.44 ℃,

resulting in a 6.01% mass loss. The second stage consists of two steps: water removal and biopolymer degradation at 100.48–230 ℃, followed by articaine decomposition at 230–280 ℃, resulting in a mass loss of 57.66%. The third stage involves meloxicam decomposition with a 21.57% mass loss. In total, the patch experiences an 85.24% mass loss during thermal analysis. The CCGAR patch undergoes three main processes during thermal analysis, as shown on the DTG curve in Fig. 5. The first process involves the loss of moisture from the patch between 35.86 and 102.93 ℃, resulting in a mass loss of 7.42%. The second process involves the decomposition of the patch matrix and loss of water at a maximum of 184.75 ℃, causing a mass loss of 44.80%. The third process involves the decomposition of the active substances, sodium diclofenac and articaine, resulting in a mass loss of 19.55% at 274.11 ℃. Once the patch matrix decomposes, the active substances begin to decompose as well. Overall, the total mass loss is 71.77% of the initial sample mass. The data obtained from the thermogravimetric analysis of this patches are presented graphically in Fig. 5.

b. Patches in which lidocaine was combined with anti-inflammatory drugs.

The DTG curve for the CCGLD patch shows three main thermal processes with a total mass loss of 53.47%. The first process, at 37.16—90.16 ℃, is moisture loss, with a mass loss of 3.64%. The second process, at 146.89 ℃, involves the removal of water from the membrane and polysaccharide matrix with a mass loss of 23.77%. The third process, at 218.70—354.59 ℃, is the thermal decomposition of active substances with a mass loss of 26.06%. Similarly, the CCGLM patch has three thermal processes. Moisture loss occurs in the first process, with a 7.11% mass loss at 39.01–87.89 ℃. The second process involves water removal from the poly-
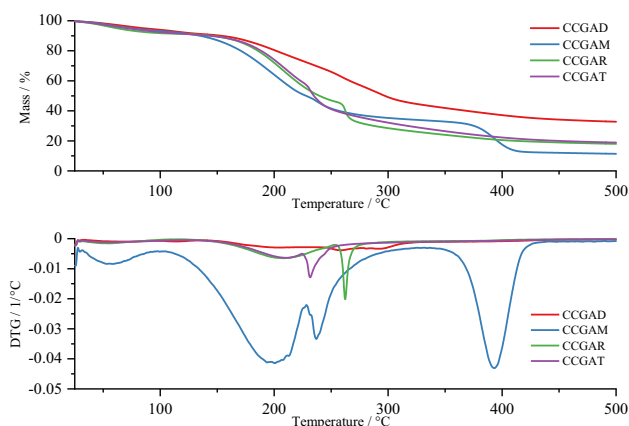

Fig. 5 TG and DTG curves for patches incorporating articaine and anti-inflammatory drugs

mer matrix, decomposition, and thermal decomposition of the local anesthetic with a mass loss of 48.12% at 192.95 ℃. The third process, above 300℃, is the decomposition of meloxicam. The CCGLR patch also goes through three processes. The first involves moisture removal with a mass loss of 5.90% at 63.25℃. The second includes water removal and decomposition with a mass loss of 41.15%. The decomposition of medicinal substances begins at 239.30 ℃ with a 22.89% mass loss at 257.08 ℃. For the CCGLT patch, there are three thermal processes with a total mass loss of 68.16%. Moisture loss in the first process is 9.33% at 40.40–108.87 ℃. The second process involves degradation of the polysaccharide matrix and water removal with a mass loss of 31.93% at 186.22 ℃. The third process, starting at 186.22 ℃ and continuing into the second process, is the thermal decomposition of both drug components with a mass loss of 26.80% at 230.02 ℃. The data obtained from the thermogravimetric analysis of this patches are presented graphically in Fig. 6.

c. Patches in which bupivacaine was combined with anti-inflammatory drugs.

The CCGBD patch experienced a total mass loss of 53.80% between 38.80 and 445.47℃. The loss occurred in multiple processes observed on the DTG curve. The first process saw a 3.56% mass loss due to water removal, while the second process had a 3.17% loss. The thermal decomposition of the patch began at 151.37℃, resulting in a continuous process involving the decomposition of the patch matrix and active substances. This led to a total mass loss of 47.07%. As for CCGBM patch, it presents three decomposition processes, resulting in an 81.36% mass loss. The first process saw a 5.45% loss due to wet losses. The second process involved the removal of water from the membrane matrix and the

decomposition of the biopolymer matrix and the local anesthetic, resulting in a 55.59% mass loss. The third process resulted in a 20.32% mass loss. The CCGBR patch underwent three thermal processes, resulting in a total mass loss of 62.67%. The first process saw a 6.34% mass loss due to water removal. The second process had the highest mass loss of 36.51% due to matrix decomposition. The third process involved the thermal decomposition of active substances, resulting in a 19.82% mass loss. The CCGBT patch had three thermal decomposition processes, resulting in a total mass loss of 59.61%. The first process saw a 4.17% loss due to moisture removal. The second process had a 24.71% mass loss due to water loss and polymer decomposition. The last process involved the decomposition of active substances, resulting in a 30.73% mass loss. The data obtained from the thermogravimetric analysis of this patches are presented graphically in Fig. 7.

d. Patches in which ropivacaine was combined with anti-inflammatory drugs.

e. For the first patch, CCGRD, thermogravimetric analysis shows that as the temperature increases from 37.07 to 439.53 ℃, 57.12% of the sample's mass is lost (Fig. 8). Moisture loss accounts for 6.45% of the mass in the first thermal process, while the degradation of the polysaccharide matrix and more water removal occurs in the second process, resulting in a mass loss of 20.25%. After the polymer matrix degrades, the active substances start decomposing continuously, with a total loss of 30.41% between 243.46 and 439.53 ℃. For the CCGRM patch, four thermal processes result in 86.24% mass loss. Moisture loss takes place from 37.00 to 98.33 ℃, contributing to 6.89% of the total loss. Decomposition of the biopolymer matrix and water removal occur in the second process from 122.15 to 230.53 ℃, leading to
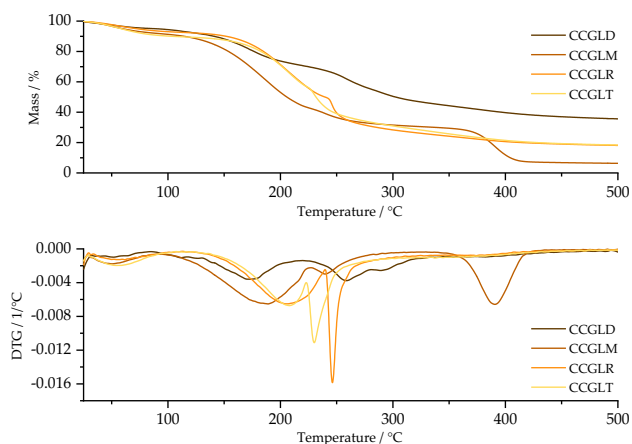

Fig. 6 TG and DTG curves for patches incorporating lidocaine and anti-inflammatory drugs
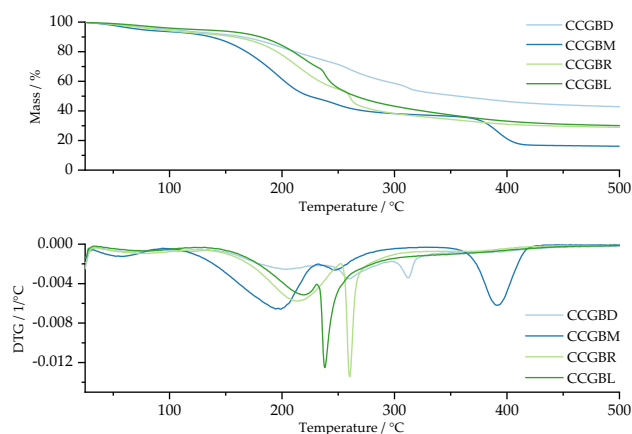

Fig. 7 TG and DTG curves for patches incorporating bupivacaine and anti-inflammatory drugs
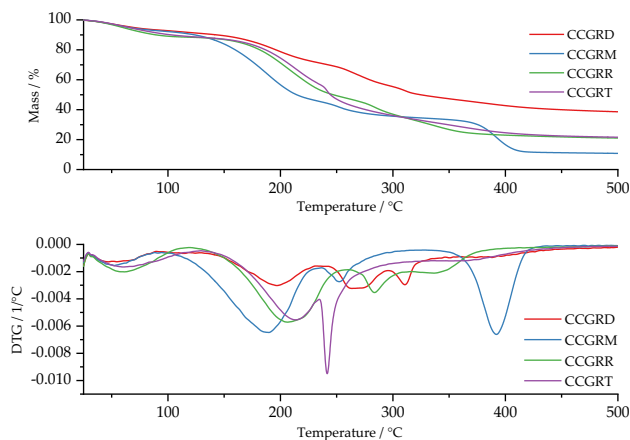
Fig. 8 TG and DTG curves for patches incorporating ropivacaine and anti-inflammatory drugs

Fig. 9 TG and DTG curves for patches incorporating mepivacaine and anti-inflammatory drugs

a 46.35% mass loss. The third process continues this decomposition and initiates the decomposition of ropivacaine, with meloxicam decomposing separately at over 300 ℃. Ropivacaine loses 11.09%, while meloxicam loses 21.91% of the sample mass. In the CCGRR patch, three thermal processes result in 74.87% mass loss. Moisture loss and matrix decomposition happen in the first two processes, with simultaneous decomposition of ropivacaine and sodium diclofenac in the third process. Finally, the CCGRT patch undergoes through three thermal processes, resulting in a total mass loss of 61.87%. Moisture is lost in the first process, "bound" water and polymer matrix decomposition in the second process, and decomposition of active substances in the third process. The data obtained from the thermogravimetric analysis of this patches are presented graphically in Fig. 8.

f. Patches in which mepivacaine was combined with anti-inflammatory drugs.

Upon closer examination of the DTG curve from the thermogravimetric analysis of the CCGMD patch in Fig. 9, it is evident that there are multiple thermal processes occurring during the decomposition. These processes involve the decomposition of the membrane matrix and medicinal components. The loss of water in the form of moisture or "bound" water, as well as the degradation of the polysaccharide matrix, exhibits observable limits. However, the decomposition of active substances seems to be a continuous thermal process with no clear boundaries. The total mass loss from the patch is 62.86%. For the CCGMD patch, the first thermal process involves the removal of moisture with a mass loss of 5.42% at 56.90 ℃. The second process involves the loss of "bound" water with a mass loss of 3.06% between 88.10 and 129.27 ℃. The decomposition of the
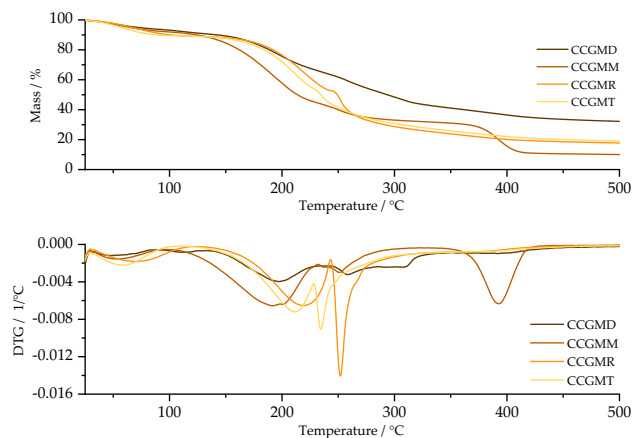
polymer membrane matrix then occurs with a mass loss of 25.11% between 133.74 and 235.69 ℃. Following this, a series of three small processes begin relating to the decomposition of active substances with a total mass loss of 29.27% between 238.87 and 438.62 ℃. The DTG curve for the CCGMM patch shows clear delineation of thermal decomposition processes for the active substances, postulated to be meloxicam and local anesthetic. Four processes can be observed with a total mass loss of 87.67%. The third process is attributed to mepivacaine and the fourth to meloxicam. For the CCGMR patch, three distinct thermal processes are observed with a total mass loss of 75.31%. The first process involves the removal of moisture while the second involves the loss of "bound" water and degradation of the polysaccharide matrix. The third process involves the decomposition of active substances. Similarly, the CCGMT patch exhibits three thermal processes with a total mass loss of 72.00%. The first process involves the removal of moisture, the second involves the decomposition of the patch matrix and removal of "bound" water, and the third involves the thermal decomposition of active substances. The data obtained from the thermogravimetric analysis of this patches are presented graphically in Fig. 9.

DSC

For the control patch (CCG), the DSC analysis highlights two endothermic effects as shown in Fig. 10. The first endothermic effect with a maximum at 115 ℃ and an enthalpy of 265.21 J·g^{-1} corresponds to the melting of the κ-carrageenan gel matrix; more precisely, we can say that in this process the liquefaction of the membrane takes place. The second thermal effect, peaking at 283 ℃, can be attributed to the melting of the plasticizer and HEC, with

Fig. 10 DSC curves for control patch (CCG) and patches incorporating dexamethasone phosphate (D) and LA
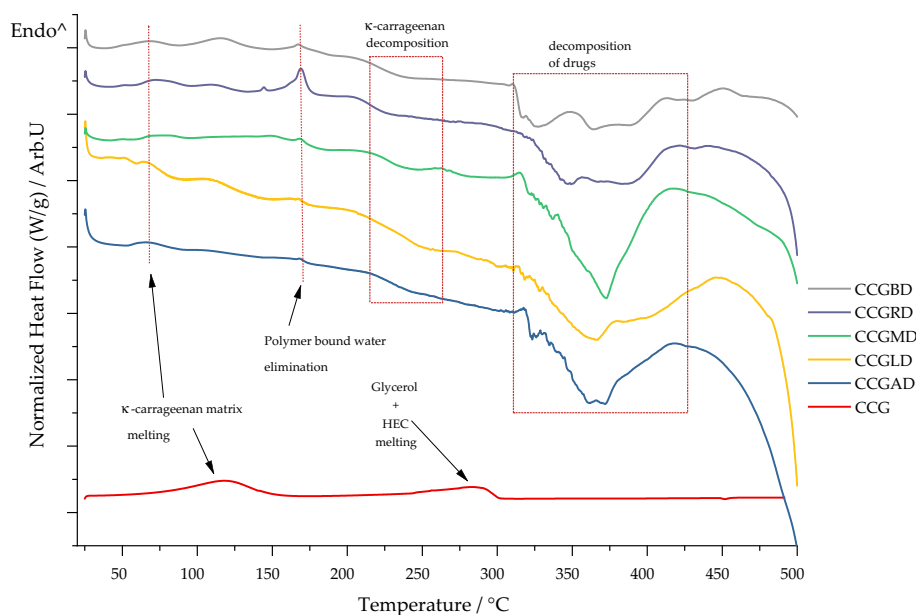
an enthalpy of 163.41 J·g^{-1}. DSC analysis indicates four distinct thermal effects for patches where dexamethasone Phosphate was combined with the five amide anesthetics. In the temperature range of 50–105 ℃, melting of the patch matrix takes place, and as can be seen, the maximum of this thermal effect is shifted to a lower temperature in contrast to its position in the case of the control patch. Thus, the lowest maximum can be found in the case of the CCGLD patch, at only 66.14 ℃, and the highest in the case of the CCGMD patch, at 76.60 ℃. Although according to Table 1, patches incorporating dexamethasone are the driest and also the most brittle, and these patches have a certain amount of water "bound" in the polymer matrix that is removed, as seen in the DSC curves appearing within the second endothermic effect at a maximum located at the temperature of ≈168 ℃. The exothermic process in which the decomposition of κ-carrageenan begins is located within the quadrant in the temperature range of 215–263 ℃, which is followed by the decomposition of HEC and glycerol. The second exothermic process from 263 to 425 ℃ corresponds to the thermal decomposition of the active substances, this effect being the most pronounced in the case of the CCGMD patch where the process enthalpy is -939.42 J·g^{-1} with a maximum located at 373.95 ℃. Therefore, the process of thermal decomposition of both the patch base and the active substances is a continuous process, because once the entire amount of biopolymers and plasticizer has been decomposed, the decomposition of the active principles also begins, within the temperature limits of 215–425 ℃, as can be seen on their DSC curves.

For the patches in which meloxicam was combined with local anesthetics, the DSC analysis data are presented in Fig. 11. The first endothermic process that can be seen on
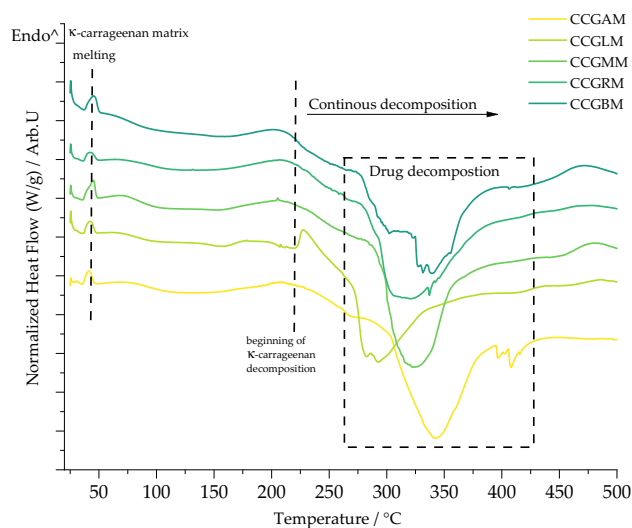

Fig. 11 DSC curves for patches incorporating meloxicam (M) and LA

all DSC curves of the meloxicam patches is attributed to the melting of the patch matrix and is located at a maximum of only 45.33 ℃. Knowing that this process is located at 115 ℃ for the control patch and 66.14 ℃ for the CCGLD sample, the temperature value for the meloxicam patches can indicate a quite interesting fact, namely, that these patches are much drier than the dexamethasone ones, even though their integrity is not being compromised by the low "bound" water content, as can be seen from their physical appearance in Table 1. The exothermic effect of the decomposition of κ-carrageenan starts at 214 ℃, similar to that of dexamethasone patches, and the decomposition of HEC and glycerol being contained within it, their limits not being easily

observable. With the completion of this continuous decomposition, the decomposition of the active substances also begins, with a variation in the maximum value of this thermal effect depending on the analyzed patch. Thus, the highest value of this thermal effect can be found in the CCGAM patch, 343.66 ℃, and the lowest value in the CCGLM sample, 288.167 ℃. The highest enthalpy value for this exothermic effect is 821.38 J·g^{-1}, for the CCGMM sample, and the lowest for the CCGBM sample, namely 548.76 J·g^{-1}. A particular case can be found in the CCGLM sample; namely, an endothermic effect that precedes the decomposition of the active substances is nothing more than the crystallization of the active substances with an enthalpy of 28.29 J·g^{-1}, for a maximum of 226.50 ℃.

The DSC analysis data for patches with combinations of dexketoprofen and anesthetics are presented in Fig. 12. As before, the first thermal effect corresponds to the melting of the polysaccharide matrix with lower values than in the case of the control patch. Thus, among the analyzed patches, the CCGMT sample possesses the lowest maximum, of 72.05 ℃, while the highest value can be seen in the case of the CCGLT sample, namely 91.59 ℃. By comparing the enthalpy values for this thermal effect, the value of 28.34 J·g^{-1} for the CCGRT sample and 126.70 J·g^{-1} for CCGLT, it can be concluded that the driest patch in which dexketoprofen was incorporated is CCGRT. In the case of CCGBT, CCGLT, and CCGAT patches, the exothermic effect of the decomposition of κ-carrageenan is distinguished with certainty, at 240.83 ℃. In the case of the other two patches, this effect has no observable limits, the decomposition of the active substances starting with the completion of the carrageenan decomposition. As shown in Fig. 12, thermal effects 1,2 and 3 correspond to the crystallization of the active substances. For the CCGRT
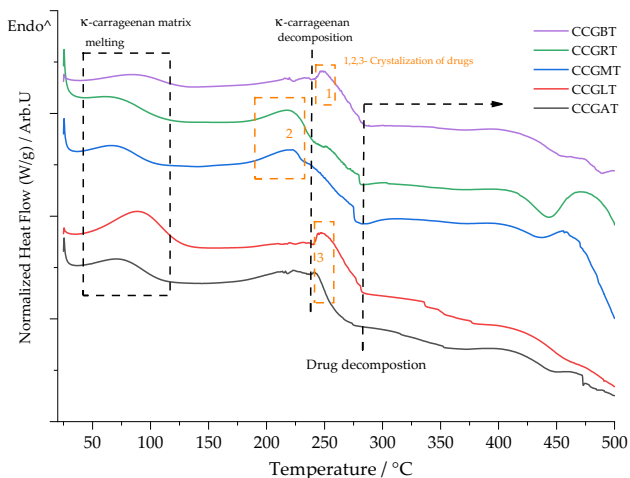
and CCGMT samples this effect is located at 219.66 ℃, before the decomposition of the carrageenan, while in the case of the CCGAT, CCGLT, and CCGBT patches, the crystallization of the active substances occurs after carrageenan decomposition. Moreover, in the case of these three patches, a drastic transition from the endothermic effect (of crystallization/melting) to the exothermic effect, that of the decomposition of medicinal compounds, can be seen. Regardless of the analyzed patch, it can be said that the decomposition of active substances starts from ≈ 274.83–279.66 ℃, mainly due to a sudden increase in the value of thermal energy in the CCGMT and CCGRT patches.

For the last five patches, in which combinations of diclofenac sodium and anesthetics were incorporated, the data obtained from the DSC analysis are presented in Fig. 13. As with the previously analyzed patches, the first thermal effect, the endothermic one, is due to the melting of the patch matrix. For diclofenac patches, the limits of this process are somewhat uniform because, as can be seen from the DSC curves, the limits are between 42.66 and 82.49 ℃. Another peculiarity expressed by diclofenac patches is the fact that the decomposition of κ-carrageenan is preceded by the crystallization of the active substances with limits between 150 and 220 ℃. The thermal effect of the decomposition of κ-carrageenan presents a maximum at ≈244.33 ℃, except for the CCGRR patch where the maximum is located at 223.83 ℃ and the CCGMR patch, namely 250.66 ℃. Regardless of the position of the maximum of the carrageenan decomposition process, once it is completed, the decomposition of the active substances begins (exothermic process), at a temperature ≥ 258 ℃.
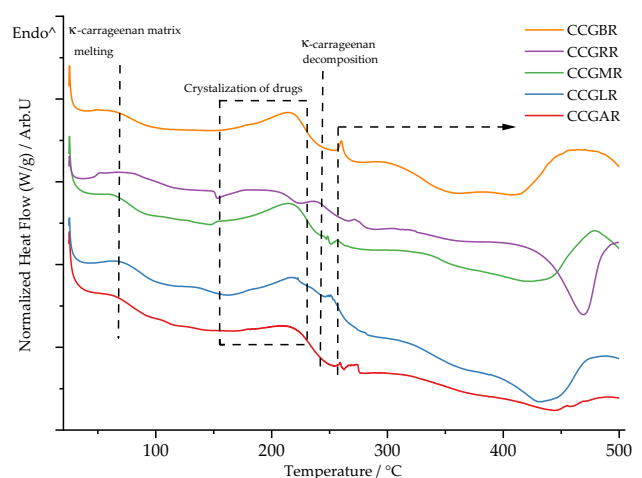

Fig. 12 DSC curves for patches incorporating dexketoprofen trometamol (T) and LA

Fig. 13 DSC curves for patches incorporating sodium diclofenac (R) and LA

Conclusions

Knowing that biopolymers represent one of the most used raw materials in the pharmaceutical industry, especially as carriers in various drug delivery systems, this study succeeded in obtaining patches that, due to their elasticity and stickiness, can be exploited in the field of transdermal delivery. Furthermore, FTIR data indicate that none of the combinations of active substances induces changes in k-carrageenan. The polymer matrix is thermally stable, between 39 and 100 ℃, indicating that they could be used as carriers of active substances, but more advanced studies must be done to obtain information on the influence of the storage temperature on the integrity and the stability of both the patch matrix and the therapeutic agents. Additionally, studies are required to identify the rate of release of the therapeutic substance, along with studies that could highlight the physical behavior of the patch and the length of its "sticky" character when applied to the skin.

Author's contribution I-AM, GV, DO, and TV conceived the study; DO, GV, I-AB, AP, and TV assisted with the methodology; I-AM, AP, and TV helped with the software; AM, DO, GV, and TV performed the validation; DO and I-AM carried out the formal analysis; AP, GV, TV, and I-AM conducted the investigation; AM, I-AB, and DO were responsible for resource; I-AB, DO, and GV curated the data; and DO, GV, and TV were involved in writing. All authors have read and agreed to the published version of the manuscript.

References

1. Wen H, Jung H, Li X. Drug delivery approaches in addressing clinical pharmacology-related issues: opportunities and challenges. AAPS Journal. 2015;17(6):1327–40. https://doi.org/10.1208/s12248-015-9814-9.
2. Tewabe A, Abate A, Tamrie M, Seyfu A, and Siraj EA, Targeted drug delivery—from magic bullet to nanomedicine: Principles, challenges, and future perspectives. J Multidiscip Healthcare 2021;14:1711–1724. Dove Medical Press Ltd. https://doi.org/10.2147/JMDH.S313968.
3. . Elsewedy HS, AlDhubiab BE, Mahdy MA, Elnahas HM, A review article on the basic concepts of drug delivery systems as targeting agents. Int J Pharma Med Biol Sci, 2021;10(1):23–29. https://doi.org/10.18178/ijpmbs.10.1.23-29.
4. Li C et al., Recent progress in drug delivery. Acta Pharm Sin B. Chinese Academy of Medical Sciences, 2019;9(6):1145–1162. https://doi.org/10.1016/j.apsb.2019.08.003.
5. Taksande JB, Gupta M, Trivedi RV, Wadher J, Umekar MJ, Formulation and characterization of organic-inorganic hybrid film for transdermal drug delivery. J Appl Pharmaceut Res., 4(3):08–15. [Online]. Available: https://media.neliti.com/media/publications/320066-formulation-and-characterization-of-orga-9c88b690.pdf
6. Galipoğlu M, Erdal MS, Güngör S. Biopolymer-based transdermal films of donepezil as an alternative delivery approach in alzheimer's disease treatment. AAPS PharmSciTech. 2014;16(2):284–92. https://doi.org/10.1208/s12249-014-0224-6.
7. Rao MG, Bharathi P, Akila RM, A comprehensive review on biopolymers. Sci Revs Chem Commun., 2014;4(2):61–68 [Online]. Available: https://www.tsijournals.com/articles/a-comprehensive-review-on-biopolymers.pdf
8. Pattanashetti NA, Heggannavar GB, Kariduraganavar MY. Smart biopolymers and their biomedical applications. Proc Manuf. 2017;12:263–79. https://doi.org/10.1016/j.promfg.2017.08.030.
9. George A, Sanjay MR, Srisuk R, Parameswaranpillai J, Siengchin S, A comprehensive review on chemical properties and applications of biopolymers and their composites. Int J Biol Macromol. 2020;154;329–338. Elsevier B.V. https://doi.org/10.1016/j.ijbiomac.2020.03.120.
10. Rebelo R, Fernandes M, Fangueiro R, Biopolymers in medical implants: a brief review. Proc Eng., 2017, pp. 236–243. Elsevier Ltd. https://doi.org/10.1016/j.proeng.2017.07.034.
11. Chakraborty S, Carrageenan for encapsulation and immobilization of flavor, fragrance, probiotics, and enzymes: a review. J Carbohydrate Chem., 2017;36(1):1–19. Taylor and Francis Inc. https://doi.org/10.1080/07328303.2017.1347668.
12. Jiang JL, Zhang WZ, Ni WX, Shao JW, Insight on structure-property relationships of carrageenan from marine red algal: a review. Carbohydrate Polym 2021;257. Elsevier Ltd. https://doi.org/10.1016/j.carbpol.2021.117642.
13. Khotimchenko M et al., Antitumor potential of carrageenans from marine red algae. Carbohydrate Polym. 2020;246 . Elsevier Ltd. https://doi.org/10.1016/j.carbpol.2020.116568.
14. Pangestuti R, Kim SK, Biological activities of Carrageenan. In Advances in food and nutrition research, 2014;72:113–124. Academic Press Inc., https://doi.org/10.1016/B978-0-12-800269-8.00007-5.
15. Sedayu BB, Cran MJ, Bigger SW. A review of property enhancement techniques for carrageenan-based films and coatings. Carbohydr Polym. 2019;216:287–302. https://doi.org/10.1016/j.carbpol.2019.04.021.
16. Dong Y, Wei Z, Xue C, Recent advances in carrageenan-based delivery systems for bioactive ingredients: a review. Trends Food Sci Technol 2021;112:348–361. https://doi.org/10.1016/j.tifs.2021.04.012.
17. Barletta M, Reed R, Local anesthetics: pharmacology and special preparations. Veterinary Clinics of North America—Small Animal Practice, 2019;49(6):109–1125. https://doi.org/10.1016/j.cvsm.2019.07.004.
18. Diemunsch P. Propriétés physicochimiques des anesthésiques locaux. Prat Anesth Reanim. 2005;9(1):5–9. https://doi.org/10.1016/s1279-7960(05)83671-x.
19. Perrin SL, Bull C, Rowe R, Black S. Local anaesthetic drugs. Anaesthesia Intensive Care Med. 2023;24(1):65–70. https://doi.org/10.1016/j.mpaic.2022.10.012.
20. Shah J, Votta-Velis EG, Borgeat A, New local anesthetics. Best Pract Res Clin Anaesthesiol. 2018;32(2):179–185. https://doi.org/10.1016/j.bpa.2018.06.010.

21. Baniceru M, Manda CV, Popescu SM. Chromatographic analysis of local anesthetics in biological samples. J Pharm Biomed Anal. 2011;54(1):1–12. https://doi.org/10.1016/j.jpba.2010.07.013.

22. Gunera-Saad N. et al., Réactions d'allure immédiate aux anesthésiques locaux : démarche diagnostique et thérapeutique. Ann Dermatol Venereol, 2007;134(4)Part 1:333–336. https://doi.org/10.1016/S0151-9638(07)89186-1.

23. Cherobin ACFP, Tavares GT, Safety of local anesthetics. Anais Brasileiros de Dermatologia 2020;95(1):82–90. https://doi.org/10.1016/j.abd.2019.09.025.

24. Bindu S, Mazumder S, Bandyopadhyay U, Non-steroidal anti-inflammatory drugs (NSAIDs) and organ damage: a current perspective. Biochem Pharmacol 2020;180. Elsevier Inc. https://doi.org/10.1016/j.bcp.2020.114147.

25. Orliaguet G, Gall O, Benabess-Lambert F. Nouveautés concernant les anti-inflammatoires stéroïdiens et non stéroïdiens. Prat Anesth Reanim. 2013;17(5):228–37. https://doi.org/10.1016/j.pratan.2013.08.002.

26. Modi CM, Mody SK, Patel HB, Dudhatra GB, Kumar A, Avale M, Toxicopathological overview of analgesic and anti-inflammatory drugs in animals. J Appl Pharm Sci 2012;2(1):149–157. Accessed: Jan. 29, 2023. [Online]. Available: https://japsonline.com/admin/php/uploads/361_pdf.pdf

27. de O. Macedo L, Barbosa EJ, Löbenberg R, Bou-Chacra NA, Anti-inflammatory drug nanocrystals: state of art and regulatory perspective. Eur J Pharmaceut Sci 2021;158:105654. https://doi.org/10.1016/j.ejps.2020.105654.

28. Delgado D, Jimenez-Kairuz A, Manzo R, Vargas E, Martínez F. Apparent molar volumes of the anesthetics procaine-HCl and lidocaine-HCl in water at temperatures from 278.15 to 313.15 K. Revista Colombiana de Ciencias Químico Farmacéuticas. 2010;39:57–67.

29. Mathie A, Veale E. Therapeutic potential of neuronal two-pore domain potassium-channel modulators. Curr Opin Investig Drugs. 2007;8:555–62.

30. Sawaki K, et al. Evaluation of high-performance liquid chromatography and mass spectrometry method for pharmacokinetic study of local anesthetic ropivacaine in plasma. Biomed Res. 2009;30:319–24. https://doi.org/10.2220/biomedres.30.319.

31. Choi YJ, Han S, Chung S, Row K. Chromatographic separation of bupivacaine racemate by mathematical model with competitive Langmuir isotherm. Korean J Chem Eng. 2004;21:829–35. https://doi.org/10.1007/BF02705528.

32. Lygre H, Moe G, Nerdal W, Holmsen H. Interaction of articaine hydrochloride with prokaryotic membrane lipids. Acta Odontol Scand. 2008;67:1–7. https://doi.org/10.1080/00016350802443466.

33. Zauska L, et al. Thermosensitive drug delivery system SBA-15-PEI for controlled release of nonsteroidal anti-inflammatory drug diclofenac sodium salt: a comparative study. Materials. 2021;14:1880. https://doi.org/10.3390/ma14081880.

34. Ochi M, Inoue R, Yamauchi Y, Yamada S, Onoue S, Development of meloxicam salts with improved dissolution and pharmacokinetic behaviors in rats with impaired gastric motility. Pharm Res 2012;30. https://doi.org/10.1007/s11095-012-0878-2.

35. Coban O, Degim Z, Development and validation of highly selective method for the determination of imatinib mesylate and dexketoprofen trometamol combination in three different media. Braz J Pharmaceut Sci.,2020;56 https://doi.org/10.1590/s2175-97902019000418583.

36. Hotha K. Drug-excipient interactions: case studies and overview of drug degradation pathways. Am J Analyt Chem. 2016;7:107–40. https://doi.org/10.4236/ajac.2016.71011.

37. Calvino MM, Cavallaro MM, Lazzara G, Milioto S, Talc concentration effect on shelf life of acetaminophen tablets. J Therm Anal Calorim., 2023;148:13133–13139. [Online]. Available: https://api.semanticscholar.org/CorpusID:260801946

38. Leyk E, Wesolowski M, The effect of cellulose derivatives on paracetamol crystallinity reduction. J Therm Anal Calorim., 2022;147. https://doi.org/10.1007/s10973-022-11312-9.

Publisher's Note Springer Nature remains neutral with regard to jurisdictional claims in published maps and institutional affiliations.